

# Structures of Tetrasilylmethane Derivatives (XMe<sub>2</sub>Si)<sub>2</sub>C(SiMe<sub>3</sub>)<sub>2</sub> (X = H, Cl, Br) in the Gas Phase, and their Dynamic Structures in Solution

Derek A. Wann,<sup>\*,†</sup> Matthew S. Robinson,<sup>†</sup> Karin Bätz,<sup>‡</sup> Sarah L. Masters,<sup>§</sup> Anthony G. Avent,<sup>||,⊥</sup> and Paul D. Lickiss<sup>\*,‡</sup>

<sup>†</sup>Department of Chemistry, University of York, Heslington, York, U.K. YO10 5DD

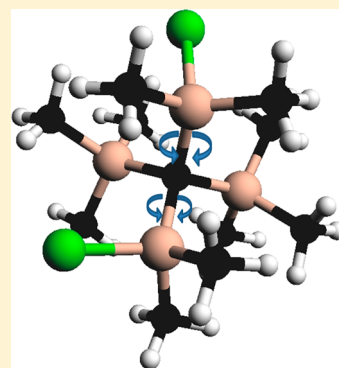
<sup>‡</sup>Department of Chemistry, Imperial College London, London, U.K. SW7 2AZ

<sup>§</sup>Department of Chemistry, University of Canterbury, Private Bag 4800, Christchurch 8140, New Zealand

<sup>||</sup>Department of Chemistry, School of Life Sciences, University of Sussex, Falmer, Brighton, U.K. BN1 9QJ

## Supporting Information

**ABSTRACT:** The structures of the molecules (XMe<sub>2</sub>Si)<sub>2</sub>C(SiMe<sub>3</sub>)<sub>2</sub>, where X = H, Cl, Br, have been determined by gas electron diffraction (GED) using the SARACEN method of restraints, with all analogues existing in the gas phase as mixtures of C<sub>1</sub>- and C<sub>2</sub>-symmetric conformers. Variable temperature <sup>1</sup>H and <sup>29</sup>Si solution-phase NMR studies, as well as <sup>13</sup>C NMR and <sup>1</sup>H/<sup>29</sup>Si NMR shift correlation and <sup>1</sup>H NMR saturation transfer experiments for the chlorine and bromine analogues, are reported. At low temperatures in solution there appear to be two C<sub>1</sub> conformers and two C<sub>2</sub> conformers, agreeing with the isolated-molecule calculations used to guide the electron diffraction refinements. For (HMe<sub>2</sub>Si)<sub>2</sub>C(SiMe<sub>3</sub>)<sub>2</sub> the calculations indicated six conformers close in energy, and these were modeled in the GED refinement.



## INTRODUCTION

The chemistry of tetrasilylmethane derivatives has been the subject of numerous studies, and many novel structures and unusual reactivities have been attributed to having four silicon centers in a sterically crowded environment.<sup>1–4</sup> The most widely studied tetrasilylmethane derivatives have the general structures (XMe<sub>2</sub>Si)<sub>4</sub>C, (Me<sub>3</sub>Si)<sub>3</sub>C SiRR'X, (PhMe<sub>2</sub>Si)<sub>3</sub>C SiRR'X, and (Me<sub>3</sub>Si)<sub>2</sub>C(SiMe<sub>2</sub>X)(SiR<sub>2</sub>Y) (where R and R' = Me, Et, Ph, etc., and X and Y = H, halide, OAc, etc.).<sup>1–5</sup>

A range of simple bis-functionalized tetrasilylmethanes (XMe<sub>2</sub>Si)<sub>2</sub>C(SiMe<sub>3</sub>)<sub>2</sub> (for example, X = H,<sup>6–9</sup> F,<sup>9–11</sup> Cl,<sup>7,9–14</sup> Br,<sup>6,7,9,15,16</sup> I,<sup>7,9,11,12,17</sup> OH,<sup>7,9,10,18,19</sup> OMe,<sup>10,20–22</sup> OAc,<sup>7,10,20</sup> O<sub>2</sub>CCF<sub>3</sub>,<sup>10–12,16,19</sup> OClO<sub>3</sub>,<sup>9</sup> OSO<sub>2</sub>CF<sub>3</sub>,<sup>9</sup> OSO<sub>2</sub>-*p*-C<sub>6</sub>H<sub>4</sub>Me,<sup>9</sup> and vinyl<sup>12,15</sup>) are known, but apart from the diol (HOMe<sub>2</sub>Si)<sub>2</sub>C(SiMe<sub>3</sub>)<sub>2</sub>,<sup>18</sup> little structural information is available for them. The structure of the permethyl species, (Me<sub>3</sub>Si)<sub>4</sub>C, has, however, been studied by NMR spectroscopy,<sup>23–27</sup> X-ray diffraction,<sup>28–30</sup> gas electron diffraction (GED),<sup>31,32</sup> computational methods<sup>33,34</sup> and vibrational spectroscopy.<sup>34</sup>

Solution-phase NMR spectroscopy has been used to probe dynamic processes in bulky tetrasilylmethane derivatives previously, for example, in C(SiMe<sub>3</sub>)<sub>2</sub>(SiMePh<sub>2</sub>)-(SiMe<sub>2</sub>ONO<sub>2</sub>),<sup>35</sup> C(SiMe<sub>3</sub>)<sub>2</sub>(SiClPh<sub>2</sub>)(SiMe<sub>2</sub>OMe),<sup>36</sup> (Me<sub>3</sub>Si)<sub>3</sub>CSiX<sub>3</sub> (X = Cl or Br),<sup>37</sup> and (PhMe<sub>2</sub>Si)<sub>3</sub>SiCl<sub>3</sub>.<sup>37</sup> GED studies have also been carried out on the tetrasilyl-

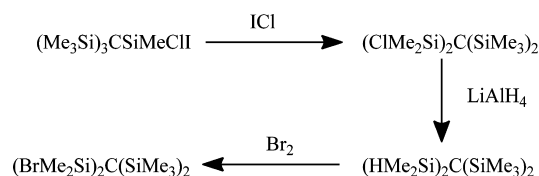
methane (Me<sub>3</sub>Si)<sub>3</sub>CSiCl<sub>3</sub><sup>38</sup> and on (HMe<sub>2</sub>Si)<sub>3</sub>CSiH<sub>3</sub>,<sup>39</sup> the latter of which showed the presence of 11 distinct conformers.

The work presented here comprises two related studies. First, the structures of (XMe<sub>2</sub>Si)<sub>2</sub>C(SiMe<sub>3</sub>)<sub>2</sub> [X = H (1), Cl (2), Br (3)] are described in the gas phase as determined by the combination of GED experiments and *ab initio* calculations, and second, NMR studies of the dynamic processes occurring for the same species in solution are presented.

## EXPERIMENTAL SECTION

**Syntheses.** The syntheses of (HMe<sub>2</sub>Si)<sub>2</sub>C(SiMe<sub>3</sub>)<sub>2</sub>,<sup>9</sup> (ClMe<sub>2</sub>Si)<sub>2</sub>C(SiMe<sub>3</sub>)<sub>2</sub>,<sup>13</sup> and (BrMe<sub>2</sub>Si)<sub>2</sub>C(SiMe<sub>3</sub>)<sub>2</sub><sup>9</sup> were carried out according to the literature methods shown in Scheme 1, and the compounds were purified for structural

**Scheme 1. Synthetic Routes to (XMe<sub>2</sub>Si)<sub>2</sub>C(SiMe<sub>3</sub>)<sub>2</sub> (X = H, Cl, Br)**



Received: November 11, 2014

Revised: January 4, 2015

studies by sublimation. Thus, treatment of  $(\text{Me}_3\text{Si})_3\text{CSiMeClI}$  with  $\text{ICl}$  leads to a rearrangement of the type often seen in tetrasilylmethane derivatives<sup>1</sup> to give  $(\text{ClMe}_2\text{Si})_2\text{C}(\text{SiMe}_3)_2$  (**2**), which is readily reduced by  $\text{LiAlH}_4$  to give  $(\text{HMe}_2\text{Si})_2\text{C}(\text{SiMe}_3)_2$  (**1**), which then affords  $(\text{BrMe}_2\text{Si})_2\text{C}(\text{SiMe}_3)_2$  (**3**) in high yield upon treatment with bromine. The fluorine analogue  $(\text{FMe}_2\text{Si})_2\text{C}(\text{SiMe}_3)_2$  can be prepared by reaction between  $(\text{AcOMe}_2\text{Si})_2\text{C}(\text{SiMe}_3)_2$  and  $\text{CsF}$ ,<sup>10</sup> while the iodine analogue  $(\text{IMe}_2\text{Si})_2\text{C}(\text{SiMe}_3)_2$  can be prepared by reaction of  $(\text{HMe}_2\text{Si})_2\text{C}(\text{SiMe}_3)_2$  and  $\text{I}_2$ ,<sup>9</sup> though neither compound was readily available for use in the current study.

**NMR Measurements.**  $^1\text{H}$ ,  $^{13}\text{C}$  and  $^{29}\text{Si}$  NMR spectra were recorded in  $\text{CDCl}_3/\text{CD}_2\text{Cl}_2$  or  $\text{CDCl}_3/\text{acetone-}d_6$  solutions using a Bruker AMX 500 spectrometer at 500, 126, and 99 MHz, respectively, unless otherwise stated. The  $^{29}\text{Si}\{^1\text{H}\}$  NMR INEPT spectra were recorded on a Bruker AMX 500 NMR spectrometer at 99 MHz, and  $^{29}\text{Si}\{^1\text{H}\}$  inverse-gated NMR spectra were recorded on a Bruker Avance 600 spectrometer at 119.23 MHz. Chemical shifts of all NMR spectra are reported in ppm relative to TMS.

All solid-state  $^{13}\text{C}\{^1\text{H}\}$  and  $^{29}\text{Si}\{^1\text{H}\}$  MAS NMR spectra were recorded on a Bruker DSX 200 WB NMR spectrometer. Samples were spun at 3–5 kHz and simple Bloch decay techniques (standard single-pulse excitation method) were used. Approximately 1000 scans per sample were collected. The operating frequencies for  $^{13}\text{C}$  and  $^{29}\text{Si}$  NMR experiments were 50.28 and 39.7 MHz, respectively.

**X-ray Crystallography.** The attempted single-crystal X-ray study for  $(\text{BrMe}_2\text{Si})_2\text{C}(\text{SiMe}_3)_2$  was carried out using an OD Xcalibur 3 diffractometer, using X-rays of wavelength 0.71073 Å, at a temperature of 100 K.

**Computational Methods.** Previous studies for similar molecules<sup>39</sup> suggested that  $(\text{XMe}_2\text{Si})_2\text{C}(\text{SiMe}_3)_2$  compounds would have a series of potential-energy minima leading to a number of conformational isomers, dependent on the relative rotations of the two  $\text{XMe}_2\text{Si}$  groups. Figure 1 shows one possible conformation of  $(\text{XMe}_2\text{Si})_2\text{C}(\text{SiMe}_3)_2$  as an illustration.

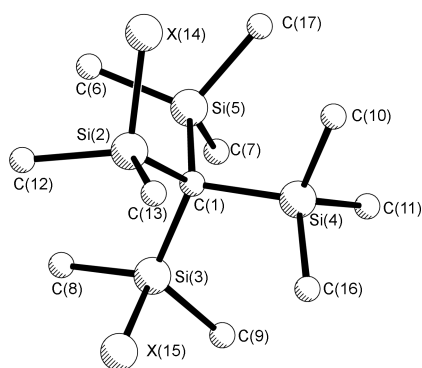


**Figure 1.** Structure, with atom numbering, of one conformer of  $(\text{XMe}_2\text{Si})_2\text{C}(\text{SiMe}_3)_2$ . Hydrogen atoms have been removed for clarity. Atoms in subsequent conformers are numbered by adding multiples of 47 to these.

These minima occurred at three approximate  $\text{X}(14/15)\text{--Si}(2/3)\text{--C}(1)\text{--Si}(3/2)$  dihedral angles: 80,  $-40$  and  $-160^\circ$ . By independently setting the two  $\text{XMe}_2\text{Si}$  to all possible combinations of these angles, it can be seen that there are nine ( $=3^2$ ) possible minimum-energy conformers for each of **1–3**. Experience of studying a similar set of species  $(\text{XMe}_2\text{Si})_4\text{C}$ ,

where  $\text{X} = \text{H}, \text{F}, \text{Cl}, \text{Br}$ , has shown that the opposite sense of each angle (i.e.,  $-80$ ,  $+40$ , and  $+160^\circ$ ) should also be considered when looking to identify all possible conformers.<sup>40</sup>

All calculations used Gaussian 09<sup>41</sup> on either the University of Edinburgh's ECDF cluster<sup>42</sup> or the UK's National Service for Computational Chemistry Software clusters.<sup>43</sup> Geometry optimizations and frequency calculations were carried out to determine which ground-state conformers had the lowest energies. For comparison, both the B3LYP<sup>44–46</sup> and M06-2X<sup>47</sup> methods with the 6-31G(d)<sup>48,49</sup> basis set were used for these calculations.

Further geometry optimizations and frequency calculations were carried out on conformers deemed to have low lying energies. The B3LYP hybrid method with the aug-cc-pVDZ basis set<sup>50,51</sup> was used for **1** and **2**, while the pseudopotential basis set aug-cc-pVDZ-PP<sup>52,53</sup> was used for **3**. These basis sets will be denoted as aug-cc-pVDZ(-PP) from hereon in. As a comparison, geometry optimizations were performed for every conformer using the M06-2X method and the aug-cc-pVDZ(-PP) basis set, as well as calculations using the MP2 method<sup>54</sup> with the 6-31G(d) and aug-cc-pVDZ(-PP) basis sets. The relative amounts of each conformer that would be present in the GED samples at the temperature of each experiment were calculated using the Gibbs free energy for each conformer (obtained from quantum calculations carried out at 0 K) and the Boltzmann distribution equation:

$$\frac{N_i}{N} = \frac{g_i \exp\left(-\frac{\Delta G_i}{RT}\right)}{\sum_i g_i \exp\left(-\frac{\Delta G_i}{RT}\right)}$$

where  $N$  is the total number of molecules, and  $N_i$  is the number of molecules in a given state  $i$ , at temperature  $T$ .  $R$  is the gas constant, while  $\Delta G_i$  and  $g_i$  are the Gibbs free energy difference (with respect to the lowest energy conformer) and degeneracy, respectively, of state  $i$ , where  $g_i$  is equal to 1 for  $C_1$  symmetric, and 2 for  $C_2$  symmetric molecules.

**Gas Electron Diffraction (GED).** Data for **1**, **2**, and **3** were collected using the GED apparatus that was used in Edinburgh until 2010.<sup>55</sup> An accelerating potential of 40 keV was applied, producing electrons with an approximate wavelength of 6.0 pm. Each molecule was analyzed with two different nozzle-to-camera distances, increasing the range of data collected. Exact nozzle-to-camera distances were calibrated by analyzing the results of benzene diffraction experiments that were carried out immediately after collecting data for the molecules of interest. The scattering intensities were recorded on Kodak Electron Image films, and measured with the use of an Epson Expression 1680 Pro flat-bed scanner and converted to mean optical densities using a method described elsewhere.<sup>56</sup> A full list of experimental parameters, including the measured nozzle and sample temperatures for each experiment, can be found in Table S1, Supporting Information.

The data were analyzed using the ed@ed least-squares refinement program v3.0,<sup>57</sup> incorporating the scattering factors of Ross et al.<sup>58</sup> Weighting points for the off-diagonal weight matrices, and scale factors can be found in Table S1, while Tables S2–S4 show the correlation matrices.

## RESULTS AND DISCUSSION

**Gas-Phase Static Structures.** By starting geometry optimization for structures with all possible combinations of minimum-energy dihedral angles, six unique conformers were

identified. Frequency calculations, carried out using M06-2X/6-31G(d) and B3LYP/6-31G(d), suggested that all of the unique conformers of **1** had similar ground-state energies, and hence all could be present in the gas phase at the temperature of the experiments. Three of these conformers have  $C_1$  symmetry (**1a–c**), and three have  $C_2$  symmetry (**1d–f**). The calculations also suggested that for **2** and **3** four of these six conformers were likely to be observable in the gas electron diffraction experiments. For each of these molecules, two conformers have  $C_1$  symmetry (**2a/b** and **3a/b**) and two have  $C_2$  symmetry (**2c/d** and **3c/d**). Tables 1–3 show the zero-point-corrected

**Table 1. Indicative Dihedral Angle, Symmetry, Relative Energy, and Proportion for Each Conformer of **1**<sup>a</sup>**

conformer	indicative dihedral angle <sup>b</sup>	point-group symmetry	relative energy <sup>c</sup>	proportion <sup>d</sup>
<b>1a</b>	−160/−40	$C_1$	1.47	0.204
<b>1b</b>	−160/80	$C_1$	0.00	0.311
<b>1c</b>	80/−40	$C_1$	0.31	0.285
<b>1d</b>	−160/−160	$C_2$	4.13	0.048
<b>1e</b>	80/80	$C_2$	2.18	0.083
<b>1f</b>	−40/−40	$C_2$	2.87	0.069

<sup>a</sup>Calculations performed using B3LYP/aug-cc-pVDZ. <sup>b</sup>These are the starting values of the H(14)–Si(2)–C(1)–Si(3)/H(15)–Si(3)–C(1)–Si(2) dihedral angles in degrees; no interconversion was observed upon optimization. See Figure 1 for atom numbering. <sup>c</sup>Gibbs free energy in kJ mol<sup>−1</sup> (ZPE corrected). <sup>d</sup>Calculated at 431 K.

**Table 2. Indicative Dihedral Angle, Symmetry, Relative Energy, and Proportion for Each Conformer of **2**<sup>a</sup>**

conformer	indicative dihedral angle <sup>b</sup>	point-group symmetry	relative energy <sup>c</sup>	proportion <sup>d</sup>
<b>2a</b>	−160/−40	$C_1$	0.00	0.720
<b>2b</b>	−160/80	$C_1$	7.56	0.106
<b>2c</b>	−160/−160	$C_2$	6.19	0.075
<b>2d</b>	80/80	$C_2$	5.07	0.099

<sup>a</sup>Calculations performed using B3LYP/aug-cc-pVDZ. <sup>b</sup>These are the starting values of the Cl(14)–Si(2)–C(1)–Si(3)/Cl(15)–Si(3)–C(1)–Si(2) dihedral angles in degrees; no interconversion was observed upon optimization. See Figure 1 for atom numbering. <sup>c</sup>Gibbs free energy in kJ mol<sup>−1</sup> (ZPE corrected). <sup>d</sup>Calculated at 485 K.

**Table 3. Indicative Dihedral Angle, Symmetry, Relative Energy, and Proportion for Each Conformer of **3**<sup>a</sup>**

conformer	indicative dihedral angle <sup>b</sup>	point-group symmetry	relative energy <sup>c</sup>	proportion <sup>d</sup>
<b>3a</b>	−160/−40	$C_1$	0.00	0.785
<b>3b</b>	−160/80	$C_1$	8.76	0.086
<b>3c</b>	−160/−160	$C_2$	8.63	0.044
<b>3d</b>	80/80	$C_2$	6.07	0.085

<sup>a</sup>Calculations performed using B3LYP/aug-cc-pVDZ-PP. <sup>b</sup>These are the starting values of the Br(14)–Si(2)–C(1)–Si(3)/Br(15)–Si(3)–C(1)–Si(2) dihedral angles in degrees; no interconversion was observed upon optimization. See Figure 1 for atom numbering. <sup>c</sup>Gibbs free energy in kJ mol<sup>−1</sup> (ZPE corrected). <sup>d</sup>Calculated at 486 K.

ground-state Gibbs free energies for all conformers of **1**, **2**, and **3**, as obtained from the B3LYP/aug-cc-pVDZ(-PP) calculations, and relate these to the relative abundance of each conformer at the temperature of the experiment, which for each species **1–3** is an average of the recorded temperatures for both nozzle and sample (seen in Table S1) at both camera distances.

The geometry optimizations showed that the four silyl branches surrounding the central carbon atom were arranged in a near-tetrahedral formation. In order to refine the experimental GED data, parametrized models were written in FORTRAN for each of **1–3**, describing all conformers of each species that were likely to appear in the sample. The parameters used in the models were based on the bond lengths and angles of the most abundant conformer of each species, due to the small difference (less than 0.5 pm) as suggested by the MP2/aug-cc-pVDZ(-PP) geometry optimizations, for the equivalent atomic distances between the conformers. Slight deviations in bond lengths and angles between different conformers were accounted for by applying fixed (nonrefinable) differences to the parameters. For **1**, **2**, and **3**, 32, 26, and 26 parameters were used to describe six, four, and four conformers, respectively. A full and complete description of the models used to describe the molecules can be found in the Supporting Information, with full atomic coordinates for each conformer **1–3** can be found in Tables S5–S7.

Refinements of the experimental data were carried out using the SARACEN method,<sup>59–61</sup> with adjustments made for the effects of vibrational motions using data from SHRINK.<sup>62</sup> SARACEN restraint values were based on the MP2/aug-cc-pVDZ(-PP) calculations, while the ranges of values from a series of geometry optimizations were used to estimate the uncertainties in these values.

Of the parameters, 27, 22, and 20 parameters were restrained, for **1–3**, respectively, while the rest refined freely. In each model, parameters  $p_1–p_6$  describe distances between pairs of atoms in the molecule, parameters  $p_7–p_{14}$  are bond angles used to position atoms relative to one another, while parameters  $p_{15}–p_{26}$  (and additionally  $p_{27}–p_{32}$  for **1**) are sets of dihedral angles to position the four main branches in each molecule relative to each other. Tables S8–S10 contain full lists of parameters and values for each of **1–3**, respectively.

To refine the amplitudes of vibration, the individual atomic distance that produced the largest scattering effect under a particular peak was selected. All other atomic distances under that same peak (not including distances related to hydrogens on a methyl group) had their amplitudes of vibration tied to the selected amplitude at the calculated ratio, with the single amplitude being refined. For **1**, **2**, and **3**, 11, nine, and 11 amplitudes, respectively, were refined, with five, one, and five of these restrained.

The refinements were initially carried out with the amount of each conformer fixed to the calculated proportions reported in Tables 1–3 for **1–3**, respectively. Once the optimal refinement was obtained with these conformer amounts, some of the values were varied in order to determine the experimental amounts of each conformer.

Full lists of interatomic distances, amplitudes of vibration, distance corrections, and SARACEN restraints for **1**, **2**, and **3** can be found in Tables S11–S13.

Parts a–c of Figure 2 show the experimentally obtained radial distribution curves for **1**, **2**, and **3**, respectively. Difference curves can also be seen underneath each radial distribution curve, showing how good a fit was obtained to the experimental data. The related molecular scattering curves for each molecule can be seen in Figure S1a–c. The  $R_G$  factors obtained for the least-squares refinements of **1**, **2**, and **3** were 6.1%, 8.7%, and 10.9%, respectively, with  $R_D$  factors (which ignore off-diagonal elements of the weight matrix) of 3.1%, 7.4%, 7.2%, respectively. Reference 63, and other references therein, gives



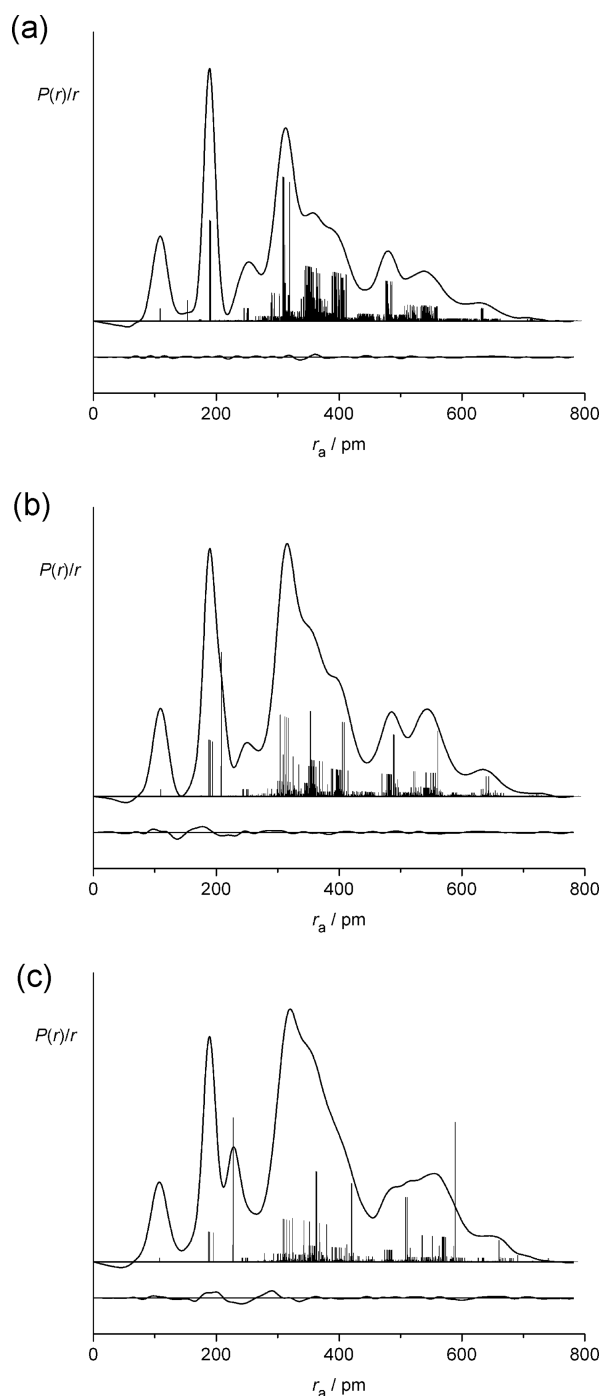


**Figure 2.** Radial distribution curves and difference curves between theoretical and experimental data for molecules **1** (a), **2** (b) and **3** (c).

a full explanation of the differences between  $R_G$  and  $R_D$ . The refined coordinates of each atom for all conformers of all three species studied can be found in Tables S14–S16.

Tables 4 and 5 contain selected parameters that demonstrate the typical bond lengths, bond angles, and dihedral angles observed for each of **1**–**3**. As the models for the GED refinement were based on the most abundant conformer of each species, with fixed differences to allow for slight deviations between that and other conformers, the bond lengths and angles relating to the main conformer are shown. However, X–Si–C–Si dihedral angles for all conformers are shown as these differ considerably between conformers of the same species.

Experimental geometric parameters are presented as  $r_{h1}$  values, which are formally derived from the vibrationally averaged  $r_a$  values that are yielded by the electron diffraction experiments (and which are listed for each pair of atoms in Supporting Information, Tables S11–S13). Vibrational corrections are applied to the  $r_a$  distances, first accounting for the amplitudes of vibration,  $u_{h1}$ , which act along the vectors between atom pairs, and then by applying the perpendicular vibrational correction,  $k_{h1}$ , which is calculated using the SHRINK program. In total this means that for any given atom pair  $r_{h1} \approx r_a + u_{h1}^2/r_a - k_{h1}$ . The  $r_e$  values quoted are determined from the theoretical equilibrium distances obtained from the various quantum chemical calculations.

For **1**, it can be seen from Table 4 that the distances to the central carbon atom, C(48) for the most abundant conformer, have a range of only around 1 pm. This is true for both the experimental and computational results. There is generally good agreement between the GED-derived distances and those from quantum chemical calculations, with the largest deviation observed for the Si–H distance. It is possible that this is due to the poor scattering ability of the lighter H atoms, but it is also likely to be a product of the anharmonicity observed in the vibration between the relatively heavy Si and light H atoms. Comparing the calculations themselves, which were all performed using the aug-cc-pVDZ basis set, both the MP2 and M06-2X theories give values that match the GED values well. The largest deviation observed relates to  $\angle C(59)$ –Si(49)–C(60), which differs by just under  $3^\circ$  from the theoretical value. However, the parameters relating to this angle have been restrained according to the SARACEN method, so we should accept this value.

For **2** and **3**, it can be seen from Table 5 that there is also reasonable agreement between calculated and experimental values. Perhaps the most striking difference between the structure of **1**, and those for **2** and **3**, is the effect of the electronegative Cl and Br atoms in the latter. For **2** and **3**, the electron withdrawing properties of atom X cause C–Si distances to the central atom to have a range of around 3 pm, and this is observed for both experimental and calculated values. Bonds to  $\text{SiMe}_3$  groups [e.g., C(1)–Si(4)] are longer than those to  $\text{SiMe}_2\text{X}$  groups [e.g., C(1)–Si(2)]; this was not observed for **1**. Again MP2 and M06-2X theories produced calculated values that are closest to the experimental values. The most significant deviations were for the Si–X distances [X = Cl (**2**), Br (**3**)], and this is likely due to the small size of the basis sets used (necessary because of computational restrictions).

As one would expect when replacing the H of **1** with the larger Cl and Br atoms in **2** and **3**, the experimentally defined angles for C(1)–Si(2)–C(12) and C(12)–Si(2)–C(13) are larger in each case than the equivalent values for **1**. Such trends are also observed from the computational results.

As mentioned before, to find all possible conformers of each of **1**–**3**, calculations were started with each  $\text{XMe}_2\text{Si}$  group set to one of three dihedral angles ( $-40^\circ$ ,  $-160^\circ$ , and  $+80^\circ$ ), and the majority of optimized dihedral angles fell within  $5^\circ$  of the expected angles. While most of the refined dihedral angles were close to the computationally predicted values, the dihedral angle  $\phi_{\text{Cl}(61)\text{--Si}(49)\text{--C}(48)\text{--Si}(50)}$  for **2**, deviated from the predicted computational range by  $5^\circ$ . However, we might expect more freedom in the range of dihedral angles.

All three theoretical methods (B3LYP, M06-2X, and MP2) gave similar dihedral angles for the same sets of atoms, with the

Table 4. Selected Experimental ( $r_{\text{hl}}$ ) and Theoretical ( $r_{\text{e}}$ ) Geometric Parameters for 1<sup>a</sup>

parameter	$r_{\text{hl}}$	$r_{\text{e}}$ B3LYP	$r_{\text{e}}$ MP2	$r_{\text{e}}$ M06-2X
rC(48)–Si(49)	190.1(6)	193.0	191.6	190.2
rC(48)–Si(51)	191.0(6)	193.6	191.8	190.5
rSi(49)–C(59)	188.7(1)	190.2	190.1	190.2
rSi(49)–H(61)	153.3(21)	150.1	150.3	149.8
rSi(51)–C(57)	189.0(1)	190.2	190.3	189.4
∠C(48)–Si(49)–H(61)	108.3(6)	107.2	107.6	107.6
∠C(48)–Si(49)–C(59)	115.2(9)	115.0	114.0	112.9
∠C(48)–Si(51)–C(57)	113.3(6)	112.7	112.2	112.1
∠C(57)–Si(51)–C(58)	107.0(7)	106.0	106.4	106.4
∠C(59)–Si(49)–C(60)	102.2(20)	105.0	105.8	106.6
ϕH(14)–Si(2)–C(1)–Si(3)	−160.2(35)	−163.7	−160.6	−159.2
ϕH(15)–Si(3)–C(1)–Si(2)	−41.2(15)	−42.5	−41.6	−42.1
ϕH(61)–Si(49)–C(48)–Si(50)	−163.9(12)	−160.0	−159.5	−159.6
ϕH(62)–Si(50)–C(48)–Si(49)	79.3(30)	75.9	76.2	78.9
ϕH(108)–Si(96)–C(95)–Si(97)	81.8(16)	78.8	78.8	78.4
ϕH(109)–Si(97)–C(95)–Si(96)	−43.3(13)	−40.0	−39.7	−40.3
ϕH(155)–Si(143)–C(142)–Si(144)	−161.5(7)	−162.7	−161.7	−162.3
ϕH(202)–Si(190)–C(189)–Si(191)	79.7(8)	77.7	78.4	78.2
ϕH(249)–Si(237)–C(236)–Si(238)	−42.6(13)	−46.8	−45.3	−45.7

<sup>a</sup>Distances ( $r$ ) are in pm, angles ( $\angle$ ) and dihedral angles ( $\phi$ ) are in degrees. Atom numbering as described in Figure 1.  $r_{\text{e}}$  values were calculated using the aug-cc-pVDZ basis set for each respective theory.

Table 5. Selected Experimental ( $r_{\text{hl}}$ ) and Theoretical ( $r_{\text{e}}$ ) Geometric Parameters for 2 (X = Cl) and 3 (X = Br)<sup>a</sup>

parameter	2				3			
	$r_{\text{hl}}$	$r_{\text{e}}$ B3LYP	$r_{\text{e}}$ MP2	$r_{\text{e}}$ M06-2X	$r_{\text{hl}}$	$r_{\text{e}}$ B3LYP	$r_{\text{e}}$ MP2	$r_{\text{e}}$ M06-2X
rC(1)–Si(2)	190.1(3)	192.7	190.8	189.7	189.6(13)	193.0	190.7	190.1
rC(1)–Si(4)	193.8(3)	196.2	193.8	192.9	195.0(13)	196.5	193.8	193.2
rSi(2)–C(12)	187.7(7)	188.7	188.6	187.6	187.4(2)	188.9	188.6	187.7
rSi(2)–X(14)	208.3(2)	215.1	213.8	213.3	227.7(2)	232.3	229.1	230.3
rSi(4)–C(10)	188.7(5)	189.9	189.7	188.8	188.7(2)	189.8	189.7	188.7
∠C(1)–Si(2)–X(14)	109.6(6)	109.5	108.2	108.6	110.6(7)	111.1	108.9	110.1
∠C(1)–Si(2)–C(12)	116.1(2)	115.6	115.4	115.3	116.3(7)	115.3	115.6	115.1
∠C(1)–Si(4)–C(10)	111.9(3)	112.8	112.1	112.1	112.0(6)	112.8	112.2	112.2
∠C(10)–Si(4)–C(11)	105.9(7)	105.5	106.1	106.0	106.0(7)	105.5	105.9	105.9
∠C(12)–Si(2)–C(13)	107.9(13)	107.4	107.9	107.7	106.8(21)	107.8	108.5	108.4
ϕX(14)–Si(2)–C(1)–Si(3)	−156.7(9)	−159.2	−158.6	−158.9	−158.7(12)	−158.9	−157.9	−158.8
ϕX(15)–Si(3)–C(1)–Si(2)	−43.2(7)	−41.8	−41.2	−41.9	−41.9(13)	−42.3	−41.1	−42.2
ϕX(61)–Si(49)–C(48)–Si(50)	−160.8(5)	−165.8	−165.6	−166.0	−163.1(11)	−166.4	−166.5	−166.8
ϕX(62)–Si(50)–C(48)–Si(49)	74.7(7)	77.6	78.0	77.6	75.7(11)	78.04	78.4	78.2
ϕX(108)–Si(96)–C(95)–Si(97)	−161.5(6)	−161.8	−161.1	−161.6	−161.3(13)	−162.0	−161.0	−161.7
ϕX(155)–Si(143)–C(142)–Si(144)	76.9(4)	75.5	75.7	75.4	76.5(8)	75.2	75.4	75.0

<sup>a</sup>Distances ( $r$ ) are in pm, angles ( $\angle$ ) and dihedral angles ( $\phi$ ) are in degrees. Atom numbering as described in Figure 1.  $r_{\text{e}}$  values were calculated using the aug-cc-pVDZ basis set for 2, and aug-cc-pVDZ-PP for 3, for each respective theory, and are based on the most abundant conformer for each molecule.

largest discrepancies being 0.7 and 1.2° between predicted values for 2 and 3, respectively. The three methods also predicted similar dihedral angles for the same set of atoms for 1, although there were some larger discrepancies between methods, with the largest being 4.5° [relating to  $\phi\text{H}(14)\text{--Si}(2)\text{--C}(1)\text{--Si}(3)$ ]. The refined dihedral angles, which were all restrained using SARACEN,<sup>59–61</sup> fell within 5° of the predicted calculations, tending also toward the expected dihedral angles.

In terms of the amount of each conformer present for each molecular species, it was found that for 1 there was little change in the  $R_{\text{G}}$  value of the refinement as the conformer ratio was adjusted. This is to be expected of 1 due to the nature of the hydrogen atoms on the silicon group, allowing for free rotation

of the SiHMe<sub>2</sub> groups. Therefore, the refinement for this species was performed with the conformers fixed at the proportions predicted in Table 1. For 2 and 3, a noticeable change in the  $R_{\text{G}}$  value was observed as the relative amounts of the two lowest energy conformers **a** and **b** (as predicted in Tables 2 and 3) were adjusted. The amounts of **c** and **d** remained fixed. How the  $R_{\text{G}}$  values vary for each of 2 and 3 is illustrated in Figure 3, which also shows the 95% confidence level (represented by a horizontal bar). For 2, a relatively shallow minimum is observed around the proportion predicted in Table 2. Because of this, the conformer ratio for 2 was kept at the values seen in Table 2 for the final refinement. For 3, a more pronounced minimum is observed in Figure 3, with the final refinement performed where the proportion of conformers

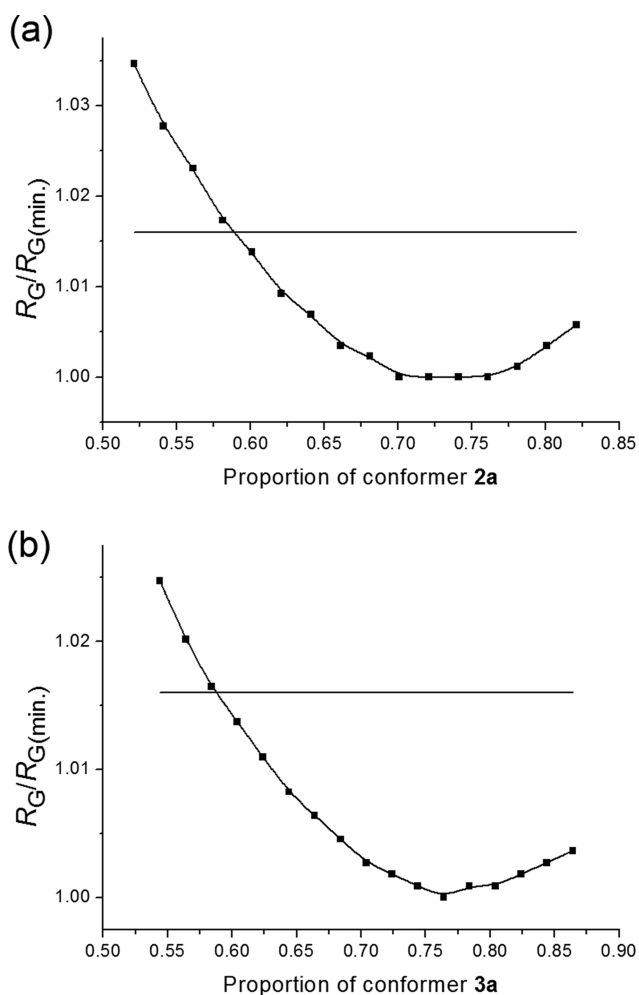


**Figure 3.** Variation in  $R_G/R_{G(\min.)}$  for (a) **2** and (b) **3** as the proportions of conformers **a** and **b** are varied relative to each other. The proportion of conformers **c** and **d** remained fixed. The horizontal bar represents the 95% confidence limit for the data.

**a:b:c:d** was 0.764:0.106:0.045:0.085. The results for **2** and **3** show that the theory was accurate in predicting the relative amounts of the most abundant conformers.

The refinements performed here for **1** can be compared to those for  $(\text{HMe}_2\text{Si})_3\text{CSiH}_3$ , 11 conformers of which are reported in ref 39. The average bond lengths observed for the various C–Si distances for  $(\text{HMe}_2\text{Si})_3\text{CSiH}_3$  [equivalent to  $r\text{C}(48)\text{--Si}(49)$  and  $r\text{Si}(49)\text{--C}(59)$  in Table 4] were 189.8 and 188.8 pm, respectively. These differ only by 0.3 and 0.1 pm, respectively, from values seen for similar bonds in **1**. Slight deviations from the angles observed for  $(\text{HMe}_2\text{Si})_3\text{CSiH}_3$  are noted for  $\angle\text{C}(48)\text{--Si}(49)\text{--C}(59)$ , with that reported in ref 39. being  $113.8(4)^\circ$ , while for **1** the value was  $115.2(9)^\circ$ . The larger angle observed in **1**, is most likely due to added strain on the branch due to larger groups around the central carbon (two  $\text{SiMe}_3$  groups and an  $\text{SiMe}_2\text{H}$  group), compared to less bulky groups (two  $\text{SiMe}_2\text{H}$  and one  $\text{SiH}_3$ ) for  $(\text{HMe}_2\text{Si})_3\text{CSiH}_3$ .

In the case of **2**, comparisons can be made with  $(\text{Me}_3\text{Si})_3\text{CSiCl}_3$ , as seen in ref 38. While the structures are quite similar, some structural differences are observed. In general, the bonds in  $(\text{Me}_3\text{Si})_3\text{CSiCl}_3$  are shorter than those in **2** by 1 to 5 pm. For example, the average distance from the central carbon atom to silicon [i.e., the mean of  $\text{C}(1)\text{--Si}(2/3/4/5)$ ] for  $(\text{Me}_3\text{Si})_3\text{CSiCl}_3$  is 190.9(8) pm, compared to 192.0

pm for **2**. The average Si–C distance for an  $\text{SiMe}_3$  branch is also shorter for  $(\text{Me}_3\text{Si})_3\text{CSiCl}_3$ , at 187.8(6) pm compared to 188.7(5) pm for **2**. The largest observed difference in bond lengths occurs with the Si–Cl distance: 203.3(6) pm for  $(\text{Me}_3\text{Si})_3\text{CSiCl}_3$ , and 208.3(2) pm for **2**. This is not surprising as the chlorine-containing moiety is quite different;  $(\text{Me}_3\text{Si})_3\text{CSiCl}_3$  exhibits stronger Si–Cl bonds than those in **2**, which is most likely due to that region being highly electronegative and drawing electrons toward it.

Differences are also observed between the two in relation to similar bond angles, with angles generally being wider for  $(\text{Me}_3\text{Si})_3\text{CSiCl}_3$  than for **2**. The C–Si–C angle in  $(\text{Me}_3\text{Si})_3\text{CSiCl}_3$  [which is equivalent to  $\angle\text{C}(10)\text{--Si}(4)\text{--C}(11)$  in **2**] is  $107.0(11)^\circ$ , compared to  $105.9(7)^\circ$  in **2**, though this difference is not significant. The biggest difference is once again for a parameter relating to the chlorine atoms. The C–Si–Cl angle [ $\angle\text{C}(1)\text{--Si}(2)\text{--Cl}(14)$ ] in  $(\text{Me}_3\text{Si})_3\text{CSiCl}_3$  is  $114.6(11)^\circ$ , while it is only  $109.6(6)^\circ$  in **2**. This may be due to the added steric hindrance of three chlorine atoms in close proximity.

**Solution-Phase Dynamic Structures.** Extensive NMR experiments were performed for **2** and **3**, with full details given in the Supporting Information.

$(\text{BrMe}_2\text{Si})_2\text{C}(\text{SiMe}_3)_2$ . The 400 MHz  $^1\text{H}$  NMR spectrum of  $(\text{BrMe}_2\text{Si})_2\text{C}(\text{SiMe}_3)_2$  (**3**) shows, as would be expected, two resonances at room temperature: a slightly broadened singlet for the  $\text{SiMe}_2\text{Br}$  protons and a sharp singlet for the  $\text{SiMe}_3$  signal (see Figure S2 in the Supporting Information). However, on lowering the temperature a much more complicated spectrum emerges and, at 213 K, the spectrum shows numerous signals in both the  $\text{SiMe}_2\text{Br}$  and  $\text{SiMe}_3$  regions (Figure S2). The  $^1\text{H}$  NMR spectrum at 201 K recorded at higher field (500 MHz, Figure S3) shows the  $\text{SiMe}_2\text{Br}$  region to have six large signals and at least six smaller signals, while the  $\text{SiMe}_3$  region has eight larger signals and at least six smaller signals together with several unidentified signals thought to belong to impurities (Figure S3). The  $^{29}\text{Si}$  NMR spectrum recorded at 300 K shows a signal at  $-0.35$  ppm, corresponding to the  $\text{SiMe}_3$  groups and a broad signal due to the  $\text{SiMe}_2\text{Br}$  region, which has begun to split out into several signals, extending from 24.38 to 22.11 ppm. These two main signals again split into numerous signals at 201 K (Figure S4) and, together with the  $^1\text{H}$  spectra, this indicates the presence of more than one conformer at low temperature.

A 2D  $^1\text{H}/^{29}\text{Si}$  NMR shift correlation spectrum of  $(\text{BrMe}_2\text{Si})_2\text{C}(\text{SiMe}_3)_2$  was recorded at 201 K in order to correlate  $^1\text{H}$  NMR signals with  $^{29}\text{Si}$  NMR signals. Each  $^{29}\text{Si}$  NMR signal in the  $\text{SiMe}_2\text{Br}$  region of the spectrum (shown in Figure 4 and Figure S5) is expected to be associated with two different proton signals. This spectrum shows that proton signals at 0.94 and 0.87 ppm, labeled A and B, correlate with the  $^{29}\text{Si}$  NMR resonance at 24.60 ppm (labeled I). The  $^{29}\text{Si}$  NMR signal at 23.40 ppm (II) is associated with proton signals C and F at 0.86 and 0.779 ppm. The third, large silicon signal III at 21.85 ppm is linked to proton signals at 0.81 ppm (D) and 0.784 ppm (E). Proton signals  $\alpha$  and  $\gamma$  concealed under a large peak at 0.86 ppm and at 0.767 ppm, correlate with the small silicon signal 1 at 24.00 ppm. Silicon signal 2 at 23.29 ppm is linked with the  $^1\text{H}$  NMR signals a and b at 0.96 ppm and hidden under a large peak at 0.779 ppm. Proton signals  $\beta$  and  $\delta$  at 0.788 and 0.74 ppm, are associated with the  $^{29}\text{Si}$  NMR signal at 20.92 ppm labeled 3.

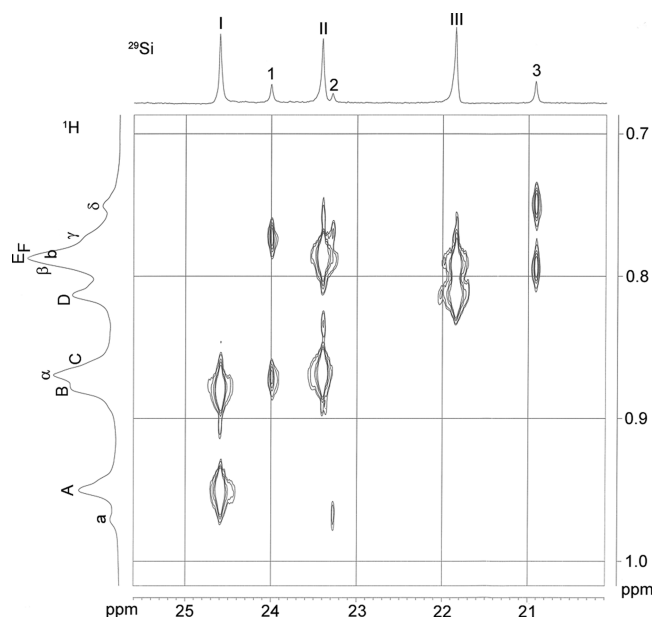


**Figure 4.** 2D  $^1\text{H}/^{29}\text{Si}$  NMR shift correlation spectrum of the  $\text{SiMe}_2\text{Br}$  region of  $(\text{BrMe}_2\text{Si})_2\text{C}(\text{SiMe}_3)_2$  in  $\text{CDCl}_3/\text{CD}_2\text{Cl}_2$  at 201 K.

As proton signals a and b are assumed to be due to a minor  $\text{C}_2$  conformer of  $(\text{BrMe}_2\text{Si})_2\text{C}(\text{SiMe}_3)_2$ , silicon signal 2 must also be associated with this conformer. Likewise, proton signals  $\alpha$ ,  $\beta$ ,  $\gamma$  and  $\delta$  assigned to minor conformer  $\text{C}_1$  are linked to silicon signals 1 and 3, which must therefore be due to the same conformer.

For the  $\text{SiMe}_3$  region of the  $^{29}\text{Si}$  NMR spectrum (see Figure 5 and Figure S6) each signal is expected to be associated with three  $^1\text{H}$  NMR signals. Interpretation of the shift correlation spectrum in a manner similar to that used for the  $\text{SiMe}_2\text{Br}$  region yields the assignments summarized in Table 6. Several small signals labeled by asterisks do not seem to correlate in a

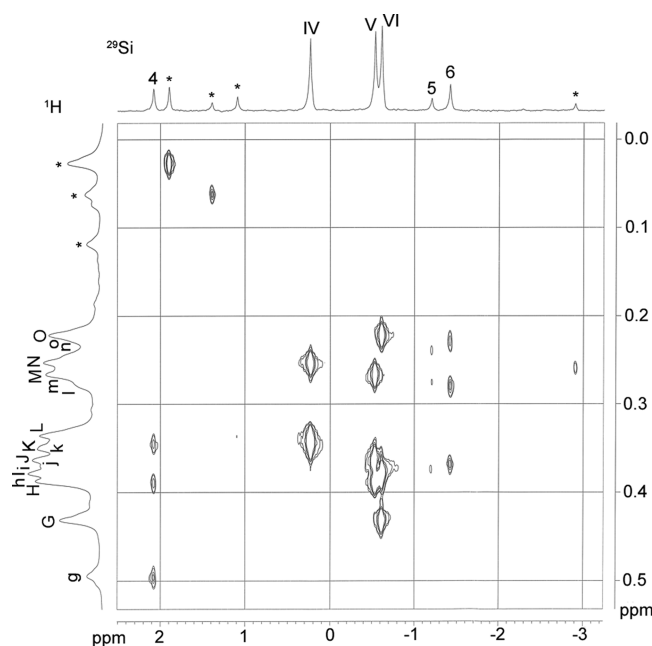


**Figure 5.** 2D  $^1\text{H}/^{29}\text{Si}$  NMR shift correlation spectrum of the  $\text{SiMe}_3$  region of  $(\text{BrMe}_2\text{Si})_2\text{C}(\text{SiMe}_3)_2$  in  $\text{CDCl}_3/\text{CD}_2\text{Cl}_2$  at 201 K. A star denotes a peak assigned to an impurity.

**Table 6.** Summary of the 2D  $^1\text{H}/^{29}\text{Si}$  NMR Shift Correlation Assignments in  $(\text{BrMe}_2\text{Si})_2\text{C}(\text{SiMe}_3)_2$

major conformers ( $\text{C}_1$ and $\text{C}_2$ )		minor conformers ( $\text{C}_1$ and $\text{C}_2$ )	
$^{29}\text{Si}$	$^1\text{H}$	$^{29}\text{Si}$	$^1\text{H}$
I	A and B	1	$\alpha$ and $\gamma$
II	C and F	2	a and b
III	D and E	3	$\beta$ and $\delta$
IV	K, L, and N	4	g, h, and k
V	H, J, and M	5	i, m, and n
VI	G, I, and O	6	j, l, and o

similar way to the  $^1\text{H}$  NMR signals and are assumed to be due to impurities which can also be seen at low intensity in the room-temperature spectra.

Several  $^1\text{H}$  NMR saturation transfer experiments on  $(\text{BrMe}_2\text{Si})_2\text{C}(\text{SiMe}_3)_2$  were recorded at 201 K to probe the exchange processes between different conformers at low temperature. Both large and small proton signals in the  $\text{SiMe}_2\text{Br}$  region of the proton spectrum were irradiated and it was clear that exchange between the major and minor conformers was occurring, but a full assignment of the enhanced signals is ambiguous in some cases due to overlap between the signals (Figure S7). Similar experiments were also carried out for the  $\text{SiMe}_3$  region signals and again while exchange processes could be observed, a full assignment could not be made (Figure S8).

A series of 126 MHz  $^{13}\text{C}\{^1\text{H}\}$  NMR spectra of  $(\text{BrMe}_2\text{Si})_2\text{C}(\text{SiMe}_3)_2$  was recorded from 293 to 213 K (Figure S9). At 293 K signals corresponding to the  $\text{SiMe}_2\text{Br}$  and  $\text{SiMe}_3$  groups, are seen at 9.89 and 4.97 ppm, respectively. As was seen for the  $^1\text{H}$  and  $^{29}\text{Si}$  spectra, the signals in the  $^{13}\text{C}$  spectrum split into a complicated pattern as the temperature is lowered (Figure S10). The signals are again consistent with the presence of major  $\text{C}_1$  and a major  $\text{C}_2$  conformers but a full analysis is hampered by the complexity and overlapping of several signals.

$(\text{ClMe}_2\text{Si})_2\text{C}(\text{SiMe}_3)_2$ . The degree of steric crowding in  $(\text{ClMe}_2\text{Si})_2\text{C}(\text{SiMe}_3)_2$  is between that of  $(\text{HMe}_2\text{Si})_2\text{C}(\text{SiMe}_3)_2$  and  $(\text{BrMe}_2\text{Si})_2\text{C}(\text{SiMe}_3)_2$  but, at readily accessible temperatures, its NMR spectra are much more similar to those of the bromide described above. Variable-temperature  $^1\text{H}$  NMR spectra are shown in Figures S11 and S12, and are reminiscent of those for  $(\text{BrMe}_2\text{Si})_2\text{C}(\text{SiMe}_3)_2$ , showing two signals at room temperature and many at low temperature. Again this is consistent with the presence of more than one conformation at low temperature. The  $^{29}\text{Si}\{^1\text{H}\}$  inverse-gated NMR spectrum of  $(\text{ClMe}_2\text{Si})_2\text{C}(\text{SiMe}_3)_2$  in  $\text{CDCl}_3$  at 300 K shows two broad resonances at 25.66 and  $-1.09$  ppm, corresponding to the  $\text{SiMe}_2\text{Cl}$  and  $\text{SiMe}_3$  groups, respectively. On lowering the temperature, these signals split into several new peaks (Figure S13), leading to numerous signals with an overall chemical shift pattern similar to that seen for  $(\text{BrMe}_2\text{Si})_2\text{C}(\text{SiMe}_3)_2$  at 201 K (see Figure S4). 2D  $^1\text{H}/^{29}\text{Si}$  NMR shift correlation spectra of  $(\text{ClMe}_2\text{Si})_2\text{C}(\text{SiMe}_3)_2$  in a  $\text{CDCl}_3/\text{acetone}-d_6$  solvent mixture were recorded at 203 K (Figures S14 and S15) and have a similar appearance to the analogous spectra for the bromide (Figures 3 and 4). However, the spectra for  $(\text{ClMe}_2\text{Si})_2\text{C}(\text{SiMe}_3)_2$  are less well resolved than for the bromide analogue and although they are consistent with the presence of a major  $\text{C}_1$  and a major  $\text{C}_2$  conformer together with minor conformers a detailed analysis has not been possible (See Supporting Information for a more detailed discussion.) Several  $^1\text{H}$  NMR saturation transfer experiments (Figures S16 and S17) at 203 K



were carried out in a similar manner to those described above for  $(\text{BrMe}_2\text{Si})_2\text{C}(\text{SiMe}_3)_2$ . The results of these saturation transfer experiments again appear to confirm that energy exchange processes at 203 K occur between small and large population conformers as well as between different low abundance conformers. It is not known what the symmetries of these conformers are. Comparison of all  $^1\text{H}$  NMR saturation transfer experiments of  $(\text{ClMe}_2\text{Si})_2\text{C}(\text{SiMe}_3)_2$  with those of the analogous compound  $(\text{BrMe}_2\text{Si})_2\text{C}(\text{SiMe}_3)_2$  show that the energy exchange processes occur, as might be expected, in similar ways in both compounds in solution at low temperature, although exchange processes between minor conformers of  $(\text{ClMe}_2\text{Si})_2\text{C}(\text{SiMe}_3)_2$  cannot be confirmed. A series of 126 MHz  $^{13}\text{C}$   $\{^1\text{H}\}$  NMR spectra of  $(\text{ClMe}_2\text{Si})_2\text{C}(\text{SiMe}_3)_2$  was also recorded from 293 to 203 K, (Figure S18 and S19). Unfortunately, the low-temperature spectra were complicated, and while they are generally consistent with the presence of the conformers described above, several peaks are not observed, presumably due to accidental signal overlap. Thus, a full analysis cannot be given. The Supporting Information provides further data and a more detailed discussion.

To summarize, at low temperatures it was possible to assign peaks in the multinuclear NMR spectra to conformers with different point-group symmetries. For example, a  $\text{C}_1$  and a  $\text{C}_2$  conformer of **2** or **3** would be expected to give rise to six and three different proton signals in the  $\text{Me}_3\text{Si}$  region, respectively. Therefore, the presence of nine large and nine small proton signals in the  $^1\text{H}$  NMR spectra recorded for **2** and **3** suggests that are two  $\text{C}_1$  and two  $\text{C}_2$  conformers are present. This is in close agreement with the results of the quantum-chemical calculations.

$(\text{HMe}_2\text{Si})_2\text{C}(\text{SiMe}_3)_2$ . Similar  $^1\text{H}$  and  $^{29}\text{Si}$  NMR spectra were recorded for  $(\text{HMe}_2\text{Si})_2\text{C}(\text{SiMe}_3)_2$  at 213 K. These, however, showed no significant changes when compared to the corresponding spectra recorded at ambient temperature. The  $^1\text{H}$  NMR spectrum at 213 K showed a singlet at 0.15 ppm ( $\text{SiMe}_3$ ), a doublet ( $\text{SiMe}_2\text{H}$ ) at 0.24 ppm and a septet ( $\text{SiMe}_2\text{H}$ ) at 4.04 ppm. Two signals were seen in the  $^{29}\text{Si}\{^1\text{H}\}$  INEPT NMR spectrum of  $(\text{HMe}_2\text{Si})_2\text{C}(\text{SiMe}_3)_2$ , one at  $-16.49$  ppm due to the  $\text{SiMe}_2\text{H}$  groups and one at  $-0.46$  ppm due to the  $\text{SiMe}_3$  groups. The proton coupled  $^{29}\text{Si}$  NMR spectrum shows complicated multiplets. The signal at  $-16.49$  ppm splits into two multiplets which selective decoupling  $^{29}\text{Si}$  DEPT NMR experiments show are due to the expected large doublet  $^1J_{\text{Si-H}}$  (182.3 Hz), a septet  $^2J_{\text{Si-H}}$  (6.4 Hz, coupling to two Me groups) and smaller doublet  $^3J_{\text{Si-H}}$  (3.2 Hz, coupling to Si-H on remote Si). The lack of dynamic processes being observed at low temperatures is presumably due to the relatively small size of H compared to the halides.

**X-ray Crystallographic Study.** Several unsuccessful attempts were made to carry out single-crystal X-ray diffraction structural analysis of  $(\text{Me}_3\text{Si})_2\text{C}(\text{SiMe}_2\text{Br})_2$  at 100 K in an attempt to freeze out any dynamic disorder present.  $(\text{Me}_3\text{Si})_2\text{C}(\text{SiMe}_2\text{Br})_2$  was determined to belong to the cubic space group  $\text{Pa}\bar{3}$  with unit cell lengths of 12.58 Å. This space group requires complete disorder of bromine positions along with at least two different sets of silicon positions. The disorder present precluded the identification of any specific conformer and no model structures could be obtained. A similar problem was noted previously for  $\text{C}(\text{SiMe}_2\text{I})_4$ , which also gave a cubic cell with  $a = 12.982(1)$  Å.<sup>64</sup>

## ■ ASSOCIATED CONTENT

### ■ Supporting Information

Additional details relating to the GED experiments (Table S1), least-squares correlation matrices (Tables S2–S4), calculated coordinated and energies (Tables S5–S7), details from the GED models and refinements, including amplitudes of vibration and curvilinear distance corrections (Tables S8–S13), final GED coordinates (Tables S14–S16), plots of molecular-scattering intensity curves (Figure S1), details of the NMR spectroscopic studies (Tables S17–S21, Figures S2–S19) and the full ref 41. This material is available free of charge via the Internet at <http://pubs.acs.org>.

## ■ AUTHOR INFORMATION

### Corresponding Authors

\*E-mail: [derek.wann@york.ac.uk](mailto:derek.wann@york.ac.uk) (D.A.W.).

\*E-mail: [p.lickiss@imperial.ac.uk](mailto:p.lickiss@imperial.ac.uk) (P.D.L.).

### Notes

<sup>†</sup>Deceased

The authors declare no competing financial interest.

## ■ ACKNOWLEDGMENTS

We thank the EPSRC for funding the electron diffraction research (EP/F037317 and EP/I004122), for partially funding, with the Chemistry Department, Imperial College, a student-ship for K.B, and for fully funding a studentship for M.S.R. The authors also wish to thank Drs. A. J. P. White and R. Law (both Imperial College) for the single-crystal X-ray crystallographic studies and solid-state NMR studies, respectively. We acknowledge the use of the E.P.S.R.C. U.K. National Service for Computational Chemistry Software (N.S.C.C.S.) hosted at Imperial College in carrying out this work, which also made use of the resources provided by the Edinburgh Compute and Data Facility (<http://www.ecdf.ed.ac.uk/>), which is partially supported by the eDIKT initiative (<http://www.edikt.org.uk>). D.A.W. thanks Prof. D. W. H. Rankin for useful discussions.

## ■ REFERENCES

- (1) Eaborn, C. Unusual Mechanistic Pathways. The Novel Chemistry of Compounds with Tris(trimethylsilyl)methyl or Related Ligands on Silicon. *J. Chem. Soc., Dalton Trans.* **2001**, 3397–3406.
- (2) Eaborn, C.; Smith, J. D. Organometallic Compounds Containing Tris(trimethylsilyl)methyl or Related Ligands. *J. Chem. Soc., Dalton Trans.* **2001**, 1541–1552.
- (3) Lickiss, P. D. *Comprehensive Organic Functional Group Transformations*; Katritzky, A. R.; Meth-Cohn, O.; Rees, C. W., Eds.; Pergamon: Oxford, U.K., 1995, Vol. 6, p377.
- (4) Lickiss, P. D. *Comprehensive Organic Functional Group Transformations II*; Katritzky, A. R.; Taylor, R. J. K., Eds.; Elsevier: Oxford, U.K., 2005, Vol. 6, p381.
- (5) Eaborn, C.; Jones, K. L.; Lickiss, P. D. Anchimeric Assistance by  $\gamma$ -aryl Groups in Reactions of Organosilicon Iodides. *J. Chem. Soc., Perkin Trans. 2* **1992**, 489–495.
- (6) Eaborn, C.; Kowalewska, A.; Smith, J. D.; Stanczyk, W. A. Anchimeric Assistance by  $\gamma$ -substituents Z, Z=MeO, PhO, MeS or PhS, in Reactions of the Bromides  $(\text{Me}_3\text{Si})_2(\text{ZMe}_2\text{Si})\text{CSiMe}_2\text{Br}$  with  $\text{AgBF}_4$ . *J. Organomet. Chem.* **2001**, 640, 29–36.
- (7) Eaborn, C.; Lickiss, P. D. Some Tetrasilylmethane Derivatives. *J. Organomet. Chem.* **1985**, 294, 305–313.
- (8) Al-Juaid, S. S.; Eaborn, C.; Habtemariam, A.; Hitchcock, P. B.; Smith, J. D. Reactions of Sterically Hindered Organozinc and Organocadmium Compounds Containing Functional Silicon Centres. Crystal Structures of  $\text{Zn}[\text{C}(\text{SiMe}_3)_2(\text{SiMe}_2\text{OCOCF}_3)]_2$  and  $\text{Cd}[\text{C}(\text{SiMe}_3)_2(\text{SiMe}_2\text{OME})]_2$ . *J. Organomet. Chem.* **1992**, 437, 41–55.



- (9) Eaborn, C.; Reed, D. E. Preparation and Reactions of Difunctional Sterically Hindered Organosilicon Compounds of the Type  $(\text{Me}_3\text{Si})_2\text{C}(\text{SiMe}_2\text{X})(\text{SiMe}_2\text{Y})$ . *J. Chem. Soc., Perkin Trans. 2* **1985**, 1687–1693.
- (10) Eaborn, C.; Lickiss, P. D.; Taylor, A. D. Reactions of the Sterically Hindered Organosilicon Diol  $(\text{Me}_3\text{Si})_2\text{C}(\text{SiMe}_2\text{OH})_2$  and Some of its Derivatives. *J. Organomet. Chem.* **1988**, 340, 283–292.
- (11) Ayoko, G. A.; Eaborn, C. Anchimeric Assistance by and Migration of the Vinyl Group in Reactions of Sterically Hindered Organosilicon Compounds of the Type  $(\text{Me}_3\text{Si})_2\text{C}(\text{SiMe}_2\text{CH}=\text{CH}_2)(\text{SiR}_2\text{X})$ . *J. Chem. Soc., Perkin Trans. 2* **1987**, 1047–1058.
- (12) Ayoko, G. A.; Eaborn, C. Reactions of Bis[dimethyl(vinyl)silyl]bis(trimethylsilyl)methane,  $(\text{Me}_3\text{Si})_2\text{C}(\text{SiMe}_2\text{CH}=\text{CH}_2)_2$ . *J. Chem. Soc., Perkin Trans. 2* **1987**, 381–383.
- (13) Eaborn, C.; Hopper, S. P. The Reactions of Tris(trimethylsilyl)silicon Iodides and Hydrides with Iodine Monochloride. *J. Organomet. Chem.* **1980**, 192, 27–32.
- (14) Seyferth, D.; Lefferts, J. L. 1,1,3,3-tetramethyl-2,2,4,4-tetrakis(trimethylsilyl)-1,3-disilacyclobutane and its 1,3-Digermene and 1,3-Distanna Analogs: Unexpected Products from the Reaction of Bis(trimethylsilyl)bromomethylithium with Dimethyldihalo Derivatives of Silicon, Germanium and Tin. *J. Organomet. Chem.* **1976**, 116, 257–273.
- (15) Damja, R. I.; Eaborn, C.; Sham, W. C. Reactions of  $(\text{Me}_3\text{Si})_3\text{CSiMe}_2\text{R}$  Compounds ( $\text{R} = \text{CH}=\text{CH}_2$ ,  $\text{CH}_2\text{CH}=\text{CH}_2$ ,  $\text{C}\equiv\text{CPh}$ ,  $\text{Ph}$ , and  $\text{CH}_2\text{Ph}$ ) with Electrophiles. *J. Organomet. Chem.* **1985**, 291, 25–33.
- (16) Eaborn, C.; Jones, K. L.; Lickiss, P. D. Reactions of Compounds of the Type  $(\text{Me}_3\text{Si})_2\text{C}(\text{SiMe}_2\text{C}_6\text{H}_4\text{Y})(\text{SiMe}_2\text{X})$  with Trifluoroacetic Acid. *J. Organomet. Chem.* **1993**, 461, 31–34.
- (17) Eaborn, C.; Jones, K. L.; Lickiss, P. D. Preparation of the Iodides  $(\text{Me}_3\text{Si})_2\text{C}(\text{SiMe}_2\text{C}_6\text{H}_4\text{Y})(\text{SiMe}_2\text{I})$  and Some Related Compounds. *J. Organomet. Chem.* **1994**, 466, 35–42.
- (18) Buttrus, N. H.; Eaborn, C.; Hitchcock, P. B.; Lickiss, P. D.; Taylor, A. D. Hydrogen Bonding in Organosilicon Hydroxides: Crystal Structures of Dicyclohexylsilanediol and Bis(hydroxydimethylsilyl)bis(trimethylsilyl)methane. *J. Organomet. Chem.* **1986**, 309, 25–33.
- (19) Eaborn, C.; Lickiss, P. D.; Ramadan, N. A. Cleavage of Silicon–Carbon Bonds in Tris(trimethylsilyl)methylsilicon Compounds by Trifluoroacetic Acid. Rearrangements and Anchimeric Assistance. *J. Chem. Soc., Perkin Trans. 2* **1984**, 267–270.
- (20) Eaborn, C.; Lickiss, P. D.; Taylor, A. D. Anchimeric Assistance by the Acetoxy Group in the Solvolysis of  $(\text{Me}_3\text{Si})_2\text{C}(\text{SiMe}_2\text{OCOMe})(\text{SiMe}_2\text{X})$ ,  $\text{X} = \text{Cl}$ ,  $\text{NCS}$  or  $\text{N}_3$ . *J. Chem. Soc., Perkin Trans. 2* **1994**, 1809–1813.
- (21) Eaborn, C.; Lickiss, P. D.; Taylor, A. D. The Nature of the Anchimeric Assistance by the Acetoxy Group in Solvolysis of  $(\text{Me}_3\text{Si})_2\text{C}(\text{SiMe}_2\text{OCOMe})(\text{SiMe}_2\text{Cl})$ . *J. Organomet. Chem.* **1988**, 338, C27–C29.
- (22) Eaborn, C.; Lickiss, P. D.; Najim, S. T.; Romanelli, M. N. 1,3-Migration of Chloride and Azide Substituents Within Organosilicon Cations, and Anchimeric Assistance by the Azido Group. *J. Organomet. Chem.* **1986**, 315, C5–C8.
- (23) Helluy, X. J.; Kummerlen, J.; Sebald, A. Comparative Solid-State NMR Study of the Molecular Dynamics of  $\text{Si}(\text{SiMe}_3)_4$  and  $\text{C}(\text{SiMe}_3)_4$ . *Organometallics* **1998**, 17, 5003–5008.
- (24) Aliev, A. E.; Harris, K. D. M.; Apperley, D. C.; Harris, R. K. Solid State Dynamic Properties of Tetrakis(trimethylsilyl)methane: High-Resolution Solid State  $^{13}\text{C}$  and  $^{29}\text{Si}$  NMR Investigations. *J. Solid State Chem.* **1994**, 110, 314–320.
- (25) Aliev, A. E.; Harris, K. D. M. Natural Abundance Solid State  $^2\text{H}$  NMR Studies of Phase Transitions in Rotator Phase Solids. *Mendeleev Commun.* **1993**, 153–155.
- (26) Wrackmeyer, B.; Zhou, H. Trimethylsilyl-, Trimethylstannyl- and Trimethylplumbylmethane Derivatives Studied by One- and Two-Dimensional Multinuclear Magnetic Resonance – Sign Inversion of the coupling constants  $^1J(^{207}\text{Pb}^{13}\text{C})$ . *Spectrochim. Acta, Part A* **1991**, 47, 849–856.
- (27) Dereppe, J. M.; Magill, J. H. Molecular Movements and Phase Transitions in Solids. Tetrakis(trimethylsilyl)methane. *J. Phys. Chem.* **1972**, 76, 4037–4039.
- (28) Lerner, H. W.; Bolte, M. Tetrakis(trimethylsilyl)methane. *Acta Crystallogr. E* **2005**, 61, 2326–2327.
- (29) Dinnebier, R. E.; Carlson, S.; van Smaalen, S. Bulk Modulus and High-Pressure Crystal Structures of Tetrakis(trimethylsilyl)methane  $\text{C}[\text{Si}(\text{CH}_3)_3]_4$  Determined by X-ray Powder Diffraction. *Acta Crystallogr. B* **2000**, 56, 310–316.
- (30) Dinnebier, R. E.; Dollase, W. A.; Helluy, X.; Kummerlen, J.; Sebald, A.; Schmidt, M. U.; Pagola, S.; Stephens, P. W.; van Smaalen, S. Order-Disorder Phenomena Determined by High-Resolution Powder Diffraction: the Structures of Tetrakis(trimethylsilyl)methane  $\text{C}[\text{Si}(\text{CH}_3)_3]_4$  and Tetrakis(trimethylsilyl)silane  $\text{Si}[\text{Si}(\text{CH}_3)_3]_4$ . *Acta Crystallogr. B* **1999**, 55, 1014–1029.
- (31) Beagley, B.; Pritchard, R. G.; Titiloye, J. O. On the  $T$  Symmetry of the Molecule Tetrakis(trimethylsilyl)methane in the Gas Phase. *J. Mol. Struct.* **1989**, 212, 323–324.
- (32) Beagley, B.; Pritchard, R. G.; Titiloye, J. O. The Molecular Structure of Tetrakis(trimethylsilyl)methane Studied by Gas-Phase Electron Diffraction and Molecular Mechanics. *J. Mol. Struct.* **1988**, 176, 81–87.
- (33) Iroff, L. D.; Mislow, K. Molecules with  $T$  symmetry. Conformational Analysis of Systems of Type  $\text{M}[\text{C}(\text{CH}_3)_3]_4$  and  $\text{M}[\text{Si}(\text{CH}_3)_3]_4$  by the Empirical Force Field Method. *J. Am. Chem. Soc.* **1978**, 100, 2121–2126.
- (34) Bürger, H.; Goetze, U.; Sawodny, W. Schwingungsspektren und Kraftkonstanten der Verbindungsklasse  $[(\text{CH}_3)_3\text{Si}]_4\text{El}^{\text{IV}}$  ( $\text{El}^{\text{IV}} = \text{C}, \text{Si}, \text{Ge}, \text{Sn}$ ). Vergleich von  $(\text{CH}_3)_3\text{Si}$ -Derivaten der 4–7. Hauptgruppe. *Spectrochim. Acta, Part A* **1970**, 26, 685–693.
- (35) Eaborn, C.; Hitchcock, P. B.; Lickiss, P. D.; Pidcock, A.; Safa, K. D. Crystal Structure and Variable-Temperature Hydrogen-1 Nuclear Magnetic Resonance Spectrum of (Dimethylnitratosilyl)-[methylphenylsilyl]bis(trimethylsilyl)methane,  $\text{C}(\text{SiMe}_3)_2(\text{SiMePh}_2)(\text{SiMe}_2\text{ONO}_2)$ . *J. Chem. Soc., Dalton Trans.* **1984**, 2015–2017.
- (36) Avent, A. G.; Lickiss, P. D.; Pidcock, A. Structure and Dynamics of Hindered Organosilicon Compounds. The Conformation and Enantiotopomerization of (Chlorodiphenylsilyl)-(methoxydimethylsilyl)bis(trimethylsilyl)methane. *J. Organomet. Chem.* **1988**, 341, 281–291.
- (37) Avent, A. G.; Bott, S. G.; Ladd, J. A.; Lickiss, P. D.; Pidcock, A. Structure and Dynamics of Hindered Organosilicon Compounds. The Conformations of Symmetrical  $(\text{Me}_3\text{Si})_3\text{C}$  and  $(\text{PhMe}_2\text{Si})_3\text{C}$  Derivatives. *J. Organomet. Chem.* **1992**, 427, 9–21.
- (38) Anderson, D. G.; Rankin, D. W. H.; Robertson, H. E.; Cowley, A. H.; Pakulski, M. Determination of the Gas-Phase Molecular Structure of Tris(trimethylsilyl)(trichlorosilyl) Methane by Electron Diffraction. *J. Mol. Struct.* **1989**, 196, 21–29.
- (39) Morrison, C. A.; Rankin, D. W. H.; Robertson, H. E.; Lickiss, P. D.; Masangane, P. C. The Synthesis of  $\text{C}[\text{Si}(\text{CH}_3)_2\text{X}]_3\text{SiX}_3$  Compounds ( $\text{X} = \text{H}, \text{Cl}, \text{Br}$  and  $\text{OH}$ ) and the Molecular Structure of  $\text{C}[\text{Si}(\text{CH}_3)_2\text{H}]_3\text{SiH}_3$  in the Gas Phase; a Study by Electron Diffraction and *ab Initio* Molecular Orbital Calculations. *J. Chem. Soc., Dalton Trans.* **1999**, 2293–2302.
- (40) Wann, D. A.; Young, S.; Bätz, K.; Masters, S. L.; Avent, A. G.; Rankin, D. W. H.; Lickiss, P. D. Structures of Tetrasilylmethane Derivatives  $\text{C}(\text{SiXMe}_2)_4$  ( $\text{X} = \text{H}, \text{F}, \text{Cl}, \text{Br}$ ) in the Gas Phase and their Dynamic Structures in Solution. *Z. Naturforsch. B* **2014**, 69, 1321–1332.
- (41) Frisch, M. J.; Trucks, G. W.; Schlegel, H. B.; Scuseria, G. E.; Robb, M. A.; Cheeseman, J. R.; Montgomery, J. A., Jr.; Vreven, T.; Kudin, K. N.; Burant, J. C. et al. Gaussian 03, Revision C.01; Gaussian, Inc.: Wallingford, CT, 2004. See Supporting Information for full reference text.
- (42) Edinburgh Compute and Data Facility (ECDF); <http://www.ecdf.ed.ac.uk/>.
- (43) EPSRC-funded NSCCS; <http://www.nscs.ac.uk/>.

- (44) Becke, A. Density-Functional Thermochemistry. III. The Role of Exact Exchange. *J. Chem. Phys.* **1993**, *98*, 5648–5652.
- (45) Lee, C.; Yang, W.; Parr, R. Development of the Colle-Salvetti Correlation-Energy Formula into a Functional of the Electron Density. *Phys. Rev. B* **1988**, *37*, 785–789.
- (46) Miehlich, B.; Savin, A.; Stoll, H.; Preuss, H. Results Obtained with the Correlation Energy Density Functionals of Becke and Lee, Yang and Parr. *Chem. Phys. Lett.* **1989**, *157*, 200–206.
- (47) Zhao, Y.; Truhlar, D. G. The M06 Suite of Density Functionals for Main Group Thermochemistry, Thermochemical Kinetics, Non-covalent Interactions, Excited States, and Transition Elements: Two New Functionals and Systematic Testing of Four M06-Class Functionals and 12 Other Functionals. *Theor. Chem. Acc.* **2008**, *120*, 215–241.
- (48) Binkley, J.; Pople, J. A.; Hehre, W. J. Self-Consistent Molecular Orbital Methods. 21. Small Split-Valence Basis Sets for First-Row Elements. *J. Am. Chem. Soc.* **1980**, *102*, 939–947.
- (49) Gordon, M.; Binkley, J.; Pople, J. A.; Pietro, W. J.; Hehre, W. J. Self-Consistent Molecular-Orbital Methods. 22. Small Split-Valence Basis Sets for Second-Row Elements. *J. Am. Chem. Soc.* **1982**, *104*, 2797–2803.
- (50) Kendall, R.; Dunning, T. H.; Harrison, R. Electron Affinities of the First-Row Atoms Revisited. Systematic Basis Sets and Wave Functions. *J. Chem. Phys.* **1992**, *96*, 6796–6808.
- (51) Wilson, A.; van Mourik, T.; Dunning, T. H. Gaussian Basis Sets for use in Correlated Molecular Calculations. VI. Sextuple Zeta Correlation Consistent Basis Sets for Boron Through Neon. *J. Mol. Struct.* **1996**, *388*, 339–349.
- (52) Woon, D. E.; Dunning, T. H. Gaussian Basis Sets for use in Correlated Molecular Calculations. III. The Atoms Aluminum Through Argon. *J. Chem. Phys.* **1993**, *98*, 1358–1371.
- (53) Peterson, K. A.; Figgen, D.; Goll, E.; Stoll, H.; Dolg, M. Systematically Convergent Basis Sets with Relativistic Pseudopotentials. II. Small-Core Pseudopotentials and Correlation Consistent Basis Sets for the Post-d Group 16–18 Elements. *J. Chem. Phys.* **2003**, *119*, 11113–11123.
- (54) Møller, C.; Plesset, M. Note on the Approximation Treatment for Many-Electron Systems. *Phys. Rev.* **1934**, *46*, 618–622.
- (55) Huntley, C. M.; Laurenson, G. S.; Rankin, D. W. H. Gas-Phase Molecular Structure of Bis(difluorophosphino)amine, Determined by Electron Diffraction. *J. Chem. Soc., Dalton Trans.* **1980**, 954–957.
- (56) Fleischer, H.; Wann, D. A.; Hinchley, S. L.; Borisenko, K. R.; Lewis, J. R.; Mawhorter, R. J.; Robertson, H. E.; Rankin, D. W. H. Molecular Structures of  $\text{Se}(\text{SCH}_3)_2$  and  $\text{Te}(\text{SCH}_3)_2$  using Gas-Phase Electron Diffraction and *ab Initio* and DFT Geometry Optimisations. *Dalton Trans.* **2005**, 3221–3228.
- (57) Hinchley, S. L.; Robertson, H. E.; Borisenko, K. R.; Turner, A. R.; Johnston, B. F.; Rankin, D. W. H.; Ahmadian, M.; Jones, J. N.; Cowley, A. H. The Molecular Structure of Tetra-*tert*-butyldiphosphine: an Extremely Distorted, Sterically Crowded Molecule. *Dalton Trans.* **2004**, 2469–2476.
- (58) Ross, A. W.; Fink, M.; and Hilderbrandt, R. *International Tables for Crystallography*; Wilson, A. J. C., Ed.; Kluwer Academic Publishers: Dordrecht, The Netherlands, 1992, Vol. C, p245.
- (59) Mitzel, N. W.; Smart, B. A.; Blake, A. J.; Robertson, H. E.; Rankin, D. W. H. Conformational Analysis of 1,4-Disilabutane and 1,5-Disilapentane by Combined Application of Gas-Phase Electron Diffraction and *ab Initio* Calculations and the Crystal Structure of 1,5-Disilapentane at Low Temperatures. *J. Phys. Chem.* **1996**, *100*, 9339–9347.
- (60) Blake, A. J.; Brain, P. T.; McNab, H.; Miller, J.; Morrison, C. A.; Parsons, S.; Rankin, D. W. H.; Robertson, H. E.; Smart, B. A. Structure Analysis Restrained by *Ab Initio* Calculations: The Molecular Structure of 2,5-Dichloropyrimidine in Gaseous and Crystalline Phases. *J. Phys. Chem.* **1996**, *100*, 12280–12287.
- (61) Mitzel, N. W.; Rankin, D. W. H. SARACEN – Molecular Structures from Theory and Experiment: the Best of Both Worlds. *Dalton Trans.* **2003**, 3650–3662.
- (62) Sipachev, V. A. Calculation of Shrinkage Corrections in Harmonic Approximation. *J. Mol. Struct. (THEOCHEM)* **1985**, *121*, 143–151.
- (63) Masters, S. L.; Atkinson, S. J.; Hölbling, M.; Hassler, K. Gas-Phase Molecular Structure of 1,1,1,2-tetrabromo-2,2-dimethyldisilane: Theoretical and Experimental Investigation of a Super-Halogenated Disilane and Computational Investigation of the F, Cl and I Analogues. *Struct. Chem.* **2013**, *24*, 1201–1206.
- (64) Lickiss, P. D. D.Phil. Thesis, University of Sussex, 1983.